Manuscript

Proof of principle of G-APD based hybrid photodetectors

C. Joram[a,1], A. Rudge[b] and J. Séguinot[a]

[a] CERN, PH department, CH-1211 Geneva 23, Switzerland

[b] Ohio State University, Columbus, Ohio 43210, USA

Abstract

We performed a proof of principle experiment which demonstrates the suitability of pixelized Geiger mode avalanche photodiodes (G-APD) for the detection of photoelectrons at energies in the 10 keV range. A pumped UHV set-up with CsI photocathode, illuminated by a UV flash lamp, is used to generate photoelectrons of defined energy. The results indicate that G-APDs can be considered as anodes in hybrid photodetectors with the potential of improved performance compared to conventional photomultiplier tubes. The concept of a G-APD based HPD has advantages but also clear drawbacks. We discuss the particular case of the X-HPD where a G-APD based anode could lead to improved detection efficiency and timing as well as to a more cost-effective production process.

1. Introduction

The ability to detect very low light levels, usually single photons, spread over a large area, is a common requirement for Cherenkov detectors in high energy physics (HEP) and astroparticle physics experiments. Instrumenting a large (~O(10 m^2)) focal plane of a Ring Imaging Cherenkov detectors (RICH) or equipping a huge photodetector matrix of an underwater Cherenkov detector, the performance of the photodetector in terms of (integral) quantum efficiency, collection efficiency, surface coverage and noise are factors with direct impact on the physics performance of the experiment. In the last two decades, new concepts of photodetectors, so-called Hybrid Photon Detectors (HPD) [1] were developed and in some cases brought to market. They combine a vacuum photocathode, usually in semitransparent mode, with either luminescent anodes (Quasar tube [2], X-HPD [3]) or segmented silicon anodes (Pixel HPD [4], HAPD [5]). The advent of the Geiger-mode APD (G-APD), also referred to as the Silicon PMT (SiPM), marks another important step: it is the first solid state device which allows for single photon detection at room temperature.

The idea, to use a G-APD as anode of a hybrid photodetector was, to our knowledge, described for the first time in [6]. In such a configuration, the G-APD doesn't serve as photodetector but to detect photoelectrons which are accelerated from the vacuum photocathode by means of a sufficiently high voltage difference. An HPD with a G-APD based anode can in principle overcome some of the limitations of classical photomultiplier tubes, such as relatively poor collection efficiency, modest single photon sensitivity (= low peak-to-valley ratio), after pulsing and transit time spread. On the other hand, the intrinsic thermal noise rate of a G-APD, which scales with the size of the G-APD, may pose a challenge for certain applications, where a low dark noise rate is a prerequisite.

[1] Corresponding author, Christian.Joram@cern.ch

The design and operation principle of a G-APD is well described in the recent literature (see e.g. [7] for an overview). The self-quenching Geiger mode operation of a micro-pixelized APD allows to achieve very high gain ($O(10^6)$)which enables single photon detection. The quasi-analog behaviour of an array of micro-APDs, when read out in parallel, leads to impressive photon counting capability. The intrinsically very high quantum efficiency (QE) of silicon can however not yet be fully maintained in a G-APD because the placement of the quench resistors and routing of bias lines decreases the active surface.

In this article we describe the first experimental study to prove the feasibility of a G-APD based HPD concept, in the following called G-HPD. We investigate the behaviour of a commercial G-APD by exposing it to photoelectrons of variable energy and intensity. The set-up, including a short summary of the G-APD properties, is described in section 2. It allows the generation of short pulses of photoelectrons and a correlated trigger signal for the G-APD readout. We describe the measurements and results in terms of noise, response to stray light and charge spectrum and an estimate of the detection efficiency in section 3. Section 4 contains a discussion of the back scattering phenomenon which is present in conventional HPDs, which however, expectedly, doesn't play a role in G-HPDs. Finally, we sketch some geometrical concepts of photodetectors which could be realized with a G-APD based anode and discuss their advantages and weaknesses.

2. Set-up

Principle

The fabrication of a sealed HPD is a labour intensive and costly endeavour. Despite the fact that we have all required technologies available in our facility at CERN, we decided to perform the first proof of principle by means of a pumped vacuum set-up, where photoelectrons are generated by exposing a semitransparent CsI photocathode to short UV light pulses of a H_2 flash lamp. In the following we describe the set-up and its main components.

Design and characteristics of the MPPC

We use G-APDs produced by Hamamatsu, commercialized as Multi Pixel Photon Counter (MPPC), of type S10362-33-050C. The device has an active surface of 3x3 mm^2, pixelized in 60 x 60 = 3600 cells of 50 x 50 μm^2. The MPPC is mounted on a ceramic substrate of about 6 x 6.6 mm^2 area. At our request, Hamamatsu delivered two such MPPCs without the standard epoxy or gel filling, which normally protects the silicon surface and the bond wires. The very restricted range of low energy (keV) electrons in matter forbids the existence of any protection layer, even if only a few μm thick. The charge gain, when operated at the bias voltage recommended by Hamamatsu is about $7.5\cdot10^5$ at T = 25°C. The dark noise at the 0.5 photoelectron level is about 5 MHz (T = 25˚C). The S10362 has a n^+pp^+ structure and is optimized for the detection of blue light. It has a peak QE of about 45-50% at 450 nm.

Test stand

Our test stand (Fig. 1) consists of a pumped vacuum vessel with various electrical and mechanical feedthroughs. We used this set-up previously to characterize X-HPD or Timepix HPD prototypes [8]. The main components are a thin (10 nm) semitransparent CsI photocathode, pre-coated by vacuum deposition together with a 1.2 nm thick Cr conductivity layer on a CaF_2 window, and a self triggering H_2 spark lamp which produces light flashes in the deep ultraviolet (VUV) around 160 nm. The lamp sits in its own N_2 flushed compartment, separated by a MgF_2 window from the vacuum chamber. Collimators and metal mesh filters allow controlling the size of the beam spot and its intensity. A mirror, mounted on a linear motion feedthrough, directs the light on the photocathode which is maintained at negative potential (0 – 30 kV). The photoelectrons released from the cathode are accelerated towards the G-APD which is maintained at ground potential. A grounded thin hexagonal stainless steel grid (T ~ 0.95) defines a flat reference equipotential surface. The typical beam spot size at the level of the G-APD is 3.6 mm (FWHM). As G-APDs have a significant sensitivity to UV photons, the mirror is aligned such that residual UV light which traverses the semitransparent photocathode should not hit the detector. A small contribution of stray light is however visible in the data (see below). The whole set-up is pumped to a vacuum level of 10^{-5} hPa and the N_2 circuit is flushed long enough to guarantee small enough concentrations of oxygen and water, and hence a constant UV transmission.

The two G-APDs and their respective fast amplifier chips (Texas Instruments OPA 847) are mounted on a PCB. The amplifiers have a voltage gain of 30 and bandwidth 130 MHz. The output is sent to a gated charge sensitive ADC (LeCroy 1182) and read via VME bus into a PC (CAEN 2718 VME-PCI Optical Link Bridge). The system is triggered by a signal which is capacitatively derived from the self-running flash lamp at a typical rate of 40 Hz. The trigger generates also the gate for the QDC which was set to a length of 50 ns. The configuration, in which the amplifiers and G-APDs share the same PCB leads to optimal signal integrity, however it has the drawback that the heat dissipated by the amplifiers can lead to an increase of the temperature and hence the dark noise rate of the G-APDs. In a specific detector design, the G-APD should be thermally isolated from any heat sources.

3. Measurements

We performed a set of initial measurements in order to characterize the noise contributions to the signal. One source is the thermal dark noise of the G-APD which – at constant gain - varies in first approximation exponentially with the temperature and is unsynchronized with the trigger. We minimized this component by reducing the gate length of the QDC to 50 ns, accepting the possible loss of a small fraction of the signal charge and by cutting the power to the second (unused) amplifier. The second contribution comes from stray light from the H_2 lamp, which traverses the photocathode unconverted and hits the G-APD after some reflections in the vessel. Direct exposure of the G-APD to photons should not occur as the tilted mirror ensures a separation of the photon and photoelectron beams, however the collimated photon beam appears to have a halo which leads to an incomplete suppression of photons in the signal spectra. Measurements with the photocathode at 0V allow extracting these two components, which can be distinguished by displacing the mirror such that the photon beam (and its halo) is moved further away from the G-APD.

Fig. 2 shows charge spectra obtained at $U_{PC} = 0$ kV with the mirror at two positions (displaced and nominal). The spectra are fitted with a Poisson distribution $P(\mu,n)$, convoluted with Gaussians $G(P(\mu,n),x_n,\sigma_n)$, where n = 0, 1, 2, … counts the photoelectrons (0 = pedestal), x_n are the equidistant photopeak positions with $x_n = x_0 + n\cdot x_1$, and σ_n characterizes the width of the Gaussians with $\sigma_n = \sqrt{n}\cdot\sigma_1$. The width of the pedestal peak σ_0 is fitted independently. The uncorrelated dark noise contribution is described by an exponential starting at x_0 which is added to the Poisson distribution.

The upper plot of Fig. 2 shows the pedestal peak (at ~160 ADC counts), an exponential background from thermal dark noise and a single photoelectron peak from stray light. From the integration of the exponential component above 0.5 pe, a dark noise rate of 5 MHz is estimated. At the nominal mirror position, the contribution of dark noise is unchanged, however the stray light component increases and exhibits a small component of double photons (small peak at ~240 ADC counts). The Poisson fit results in 0.18 detected stray light photons per trigger.

Switching on the HV and varying the cathode potential up to -25 kV allows to measure charge spectra as shown in Fig. 3 and Fig. 4. By means of metal mesh filters, added in the optical path, the intensity of the illumination can be varied in a certain range. In Fig. 4, where on average 4.3 photoelectrons are detected per trigger, one can easily identify the peaks up to 8 pe. The dark noise contribution becomes negligible. The fact that the spectra can be fitted by a distribution of the form $P\otimes G$ is an indication that the effect of photoelectron backscattering from Silicon, which is clearly visible in the charge spectra of 'normal' HPD detectors, is suppressed (see below).

Fig. 5 shows the variation of the fit parameters of data taken at U_{PC} = 0 – 25 kV. The photon intensity is the same for all measurements. The average number of detected photoelectrons μ increases and reaches a plateau at about 8 kV, indicating constant detection efficiency. The plateau is expected from the operation principle of a G-APD. The discharge of a G-APD micro-cell will always yield the full charge $Q = C_{cell} \cdot \Delta V$, independent of the origin of the electron which initiates the avalanche (thermally created, photoeffect or ionization). This is confirmed by the fact that the position of the first photoelectron charge, x_1, does not depend on the applied HV. At values below 8 kV, the probability to create an avalanche is reduced as a consequence of the energy loss in the oxide (SiO_2) and p^+ layers on top of the high field region.

The absolute value of the electron detection efficiency can't be derived from our data, as the incident photon flux and the QE of the CsI cathode are unknown. However, by using the MPPC to detect the light which traverses the CsI cathode and by making plausible assumptions for the quantum efficiencies of the CsI photocathode and the MPPC in the wavelength range of the H_2 lamp (around 160 nm), the unknown light intensity can be eliminated from the equations. The absolute value of the electron detection efficiency can then be estimated from the measured ratio N_{pe_CsI}/N_{pe_MPPC} (see footnote for details[2]). The uncertainty is however so large that we can only confirm its compatibility with 1.

4. Discussion

The measurements described in the preceding chapter prove the feasibility of using a G-APDs as an efficient detector of low energy (photo-)electrons down to energies of about 10 keV. A main motivation of our project was the investigation of the backscattering effect, which in 'normal' HPDs with Silicon or luminous anodes poses limitations to photoelectron separation (photon counting) and detection efficiency. The phenomenon of electron backscattering from Silicon is well understood and its dependence on Z_{target} and the electron energy has been extensively measured [9]. In Silicon, the back scattering probability at relevant energies (10 – 30 kV) is in the range of η = 17 - 18 %. The energy spectrum of the backscattered electron is relatively flat for low-Z materials like Silicon and extends from 0 to the initial kinetic energy of the incident electron.

If electrons are detected with a conventional (p^+n) diode -type detector, this phenomenon leads to asymmetric charge distributions with a significant low energy shoulder extending under the pedestal distribution. The single photoelectron detection efficiency is consequently limited to

$\varepsilon = 1 - \frac{\eta}{SNR} n_{\sigma,cut}$ with SNR being the ratio of signal to noise of the single photoelectron and $n_{\sigma,cut}$ the applied threshold cut in units of the Gaussian pedestal width. A detector with SNR = 10 and $n_{\sigma,cut}$ = 4 is limited to a detection efficiency of 92.8%. For multi-photon events, the probability that all n electrons deposit their full energy in the Si detector is only $(1-\eta)^n$ which becomes noticeable as a broad quasi-continuous distribution dominating at higher n over the photopeaks.

In a G-APD based detector, we expect the effect of backscattering to be significantly reduced. Of course, backscattering occurs like in a conventional p^+n diode, however in a G-APD there is no correlation between the energy deposited in a single pixel and the charge output. Even a very small deposition of energy, when the backscattered electron keeps the major part of its kinetic energy, is sufficient to initiate the Geiger avalanche.

---

[2] The electron detection efficiency ε_{det} of the G-APD can be expressed as $\varepsilon_{det} = (N_{pe,CsI} / N_{pe,MPPC}) \cdot (QE_{MPPC}/QE_{CsI}) \cdot T_{CsI}$. The ratio of the number of detected photoelectrons was measured to be $N_{pe,CsI} / N_{pe,MPPC}$ = 3.1/15 = 0.21. The transparency of the CsI layer, including the CaF_2 window, was found to be T_{CsI} = 0.62. The detection efficiency becomes then $\varepsilon_{det} = 0.13 \cdot QE_{MPPC}/QE_{CsI}$. Literature data of QE_{CsI}(160 nm) ~ 0.045 [10][11] lacks unfortunately an estimate of the precision. For the MPPC, Hamamatsu was unable to provide a value of the QE at 160 nm. For a value of ε_{det} = 1, the QE of the MPPC (at 160 nm) needs to be at least 7.8 times larger than the QE of the semitransparent CsI cathode. A value of QE_{MPPC} ~ 0.35, as required for ε_{det} = 1, appears to lie in a plausible range.

In order to extract the pure single electron charge distribution, we took data under the same experimental conditions except that in one run the HV was set to -10 kV and in the other it was switched off (see Fig. 6). Subtracting, after proper normalization, the 0 kV spectrum from the one taken at -10 kV removes the dark noise, stray light and pedestal contributions, which are identical in the two conditions, and reveals the pure photoelectron charge spectrum. The single photoelectron peak is symmetric and well described by a Gaussian. There is no indication of a backscattering shoulder. We expect therefore the detection efficiency of a G-APD based HPD to be higher than the above derived limit. In principle, it should be very close to 1.

5. Concepts of G-APD based hybrid photodetectors

We agree only partly with the authors of [6] who claim that a G-APD based vacuum phototube will overcome all the limits of a standard dynode photomultiplier and see a big potential for such tubes in fields ranging from Cherenkov based astronomy (air shower and under water/ice) through calorimetry to medical applications.
As we have just demonstrated above, the capability of a G-HPD to detect and count individual photoelectrons clearly exceeds the performance of a classical PMT. The intrinsic time resolution of a G-APD (~100 ps) is another important argument. However, when it comes to a real phototube design and construction, these advantages are to a certain extent offset by a number of limitations and constraints.
The required HV to operate a G-APD based tube will be in the 10 kV range. Special precautions in the design and fabrication of the tube are needed in order to avoid high dark noise rates from micro discharges on tube components and a degradation of the G-APD performance due to high temperature vacuum bake-out. HV values of 10 kV and above have often posed problems in cost effective internal photocathode processes during which all components are exposed to alkali vapours. The high noise count rate of G-APDs, unless operated at low temperatures, is a serious obstacle to a number of applications, where low noise count rates are mandatory. We are also less optimistic for the time resolution, since whenever photoelectrons from a large cathode surface need to be focused on a small G-APD, the time of flight fluctuations arising from different path lengths will largely dominate over the intrinsic G-APD resolution.

Less conventional designs, like the Reference concept [12] and the practically spherical design of the X-HPD which we proposed in [3] may profit most from the use of a G-APD anode (see Fig. 7). In particular, the X-HPD concept was proven to profit from a number of attractive features, such as

- very low transit time fluctuations due to the spherical design,
- high effective quantum efficiency as a consequence of a ‘double cathode effect’,
- high detection efficiency and
- insensitivity to the earth magnetic field thanks to the central E-field geometry.

We originally proposed the X-HPD with a silicon anode, consisting of small rectangular p^+n diodes forming a cube in the centre of the tube, however we built a fully operational 8-inch X-HPD tube with a luminescent anode made from a LYSO scintillator. The high effective charge number Z_{eff} of LYSO (~63) compared to Silicon (~14) resulted in a strongly increased fraction of back-scattered electrons η~50%.

Going back to the original proposal and replacing the p^+n diodes by G-APDs would bring a number of advantages:

- Firstly, the tube could operate at lower voltage (10 kV) compared to about 20 – 25 kV required to achieve sufficient gain with a p^+n diode. This would, for a simple geometry like the X-HPD, significantly increase the chance of success for an internal photocathode process.
- Secondly, the gain of the tube would be at least two orders of magnitude higher than with a p^+n diode. This, together with the reduced backscattering phenomenon, demonstrated above, would optimize the photoelectron detection efficiency.

- Finally, the superior time resolution of a G-APD compared to a p^+n diode after amplification and shaping would allow the full exploitation of the isochronicity of the electron trajectories inherent to the X-HPD concept. On the other hand, the expected multi-MHz dark noise rate of such a device could be a serious performance limitation for many applications.

In conclusion, we consider the idea of a G-APD based vacuum photodetector as a potentially interesting concept with a number of attractive features. However, in real phototube designs, some of the advantages will be masked and in particular the high dark count rate will be a serious obstacle. The X-HPD concept could profit significantly from a G-APD based anode, however the high dark count rate may again offset the performance gain.

Acknowledgements

We would like to acknowledge the excellent engineering and technical support by J. Bendotti, A. Braem, C. David and M. v. Stenis (all CERN) and E. Chesi (Ohio State University) in building the test set-up and its readout as well as in preparing the CsI photocathode. We would like to thank M. Metzger from Hamamatsu Photonics, Switzerland, for making the windowless MPPC detectors available to us and his interest in this project.

References

[1] C. Joram Nuclear Physics B (Proc. Suppl.) 78 (1999) 407-415

[2] B.K. Lubsandorzhiev, Nucl. Instr. and Meth. A 442 (2000), 368

[3] A. Braem et al. Nucl. Instr. and Meth. A 610 (2009), 61-64

[4] N. Styles et al., Nucl. Instr. and Meth. A 610 (2009), 57-60

[5] S. Nishida et al., Nucl. Instr. and Meth. A 610 (2009), 65-67

[6] G. Barbarino et al., Nucl. Instr. Meth. A 594 (2008) 326-331

[7] J. Haba, . Instr. Meth. A 595 (2008) 154-160

[8] T.K. Rügheimer et al., Nucl. Instr. Meth. A 595 (2008) *353-358*

[9] E.H. Darlington and V.E. Cosslett, J. Phys. D: Appl. Phys. 5 (1972) 1969-81 and E.H. Darlington, J. Phys. D, Vol. 8, (1975) 85-93

[10] G.R. Carruthers, Appl. Opt. 8 (1969) 633

[11] G.R. Carruthers, Appl. Opt. 20 (1981) 3693

[12] D. Ferenc et al., Nucl. Instr. Meth. A 504 (2003) *359-363*

Figure captions

Fig. 1: Schematic representation of the test stand.

Fig. 2: Upper plot: Charge spectrum at U = 0 kV, x = 80 mm, negligible stray light level. Lower plot: as above, however light spot shifted to nominal position (x = 93.5 mm)

Fig. 3: Charge spectrum at U = 25 kV. The average number of detected photoelectrons is μ = 1.45.

Fig. 4: Charge spectrum at U = 10 kV. Compared to Fig. 3, the light intensity was increased by removing one mesh filter. The average number of detected photoelectrons is μ = 4.3.

Fig. 5: Variation of measured quantities with the energy of the photoelectron. The average number of detected photoelectrons (m_Poiss) reaches a plateau at $U \geq 7.5$ kV. The position of the 1 pe peak (x1) in the charge spectrum and the width of the pedestal peak (sigma_0) do not depend on the applied acceleration voltage. The data points plotted left of the dashed line (negative U) were actually taken at U = 0 kV, with the light spot displaced by 14 mm away from the G-APD (= dark measurement).

Fig. 6: By subtracting two normalized spectra, taken at U = 10 kV (upper plot) and U = 0kV (middle plot), the pure photoelectron charge shape is extracted (lower plot). The 1 pe peak (at 195 ADC counts) is in good approximation described by a simple Gaussian. There are no indications of a low energy shoulder due to back scattering effects.

Fig. 7: Simulated field distribution and electron trajectories (SIMION 3D) in an X-HPD (8-inch diameter). The anode, made of 5 G-APDs assembled to a cube with 12 mm side length. The mechanical structure to hold the anode in the centre of the sphere is not shown in the simulation.

Figure 1

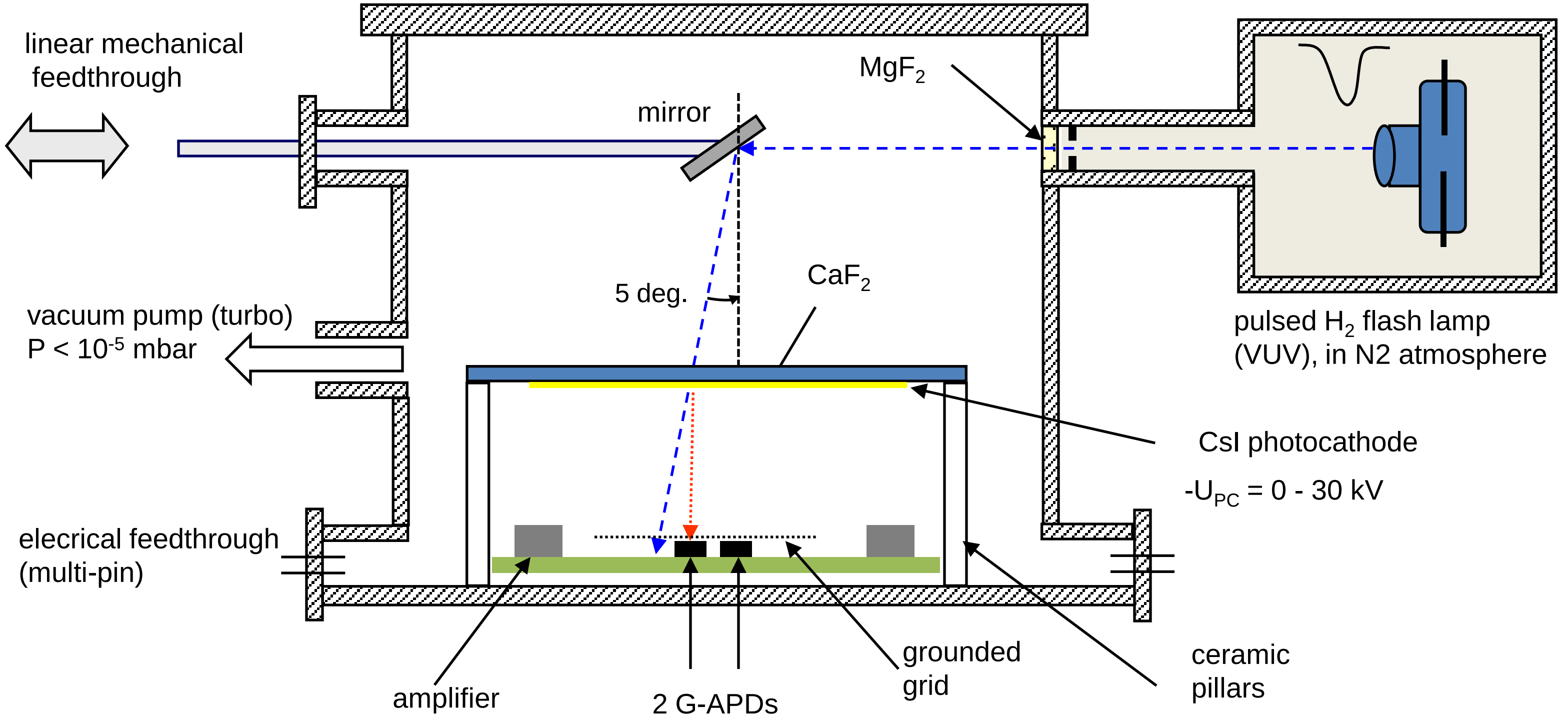

linear mechanical
feedthrough
mirror
MgF2
5 deg.
CaF2
vacuum pump (turbo)
P < 10-5 mbar
pulsed H2 flash lamp
(VUV), in N2 atmosphere
CsI photocathode
-UPC = 0 - 30 kV
elecrical feedthrough
(multi-pin)
grounded
grid
ceramic
pillars
amplifier
2 G-APDs

Figure 2

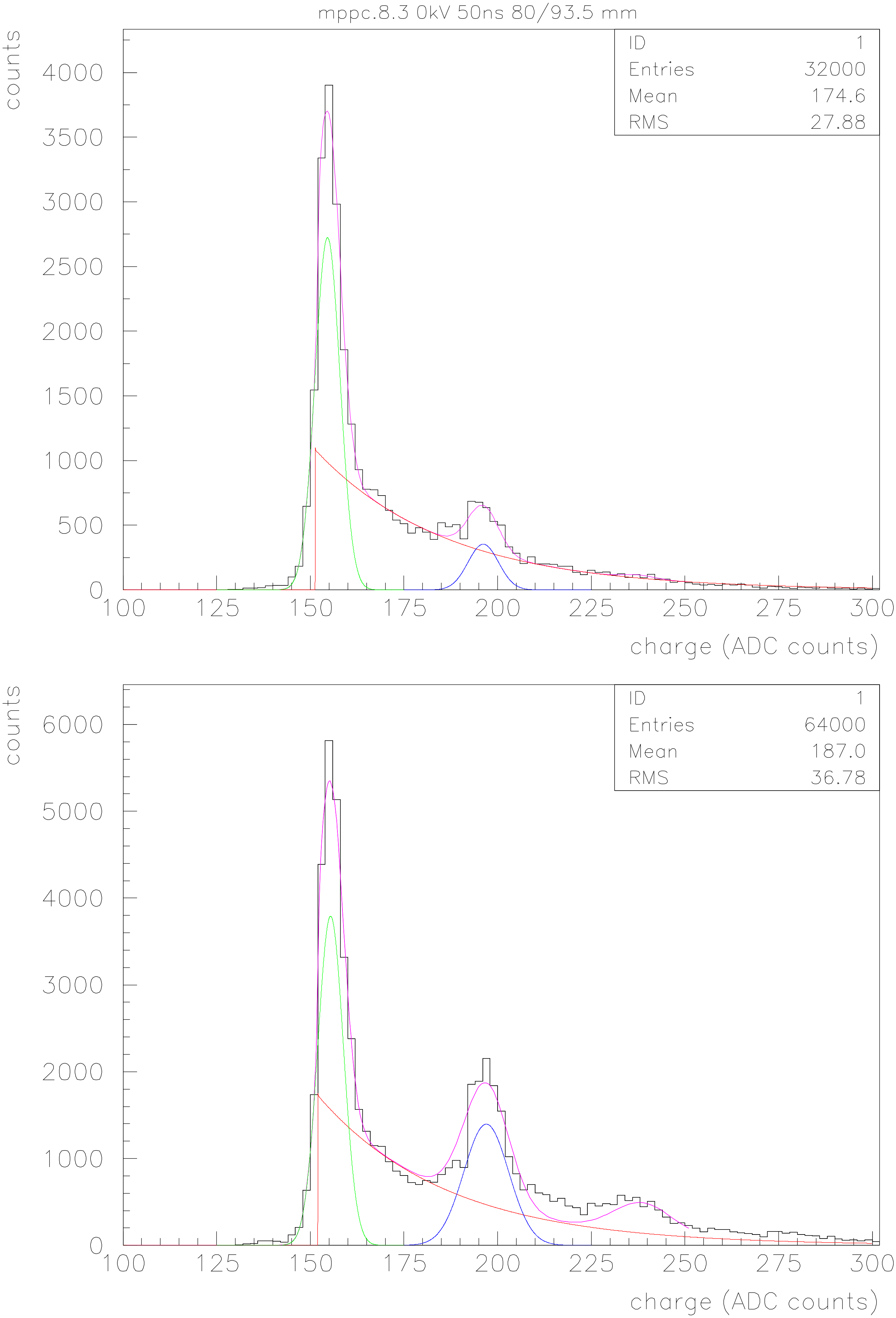

mppc.8.3 0kV 50ns 80/93.5 mm
ID 1
Entries 32000
Mean 174.6
RMS 27.88
counts
4000
3500
3000
2500
2000
1500
1000
500
0
100
125
150
175
200
225
250
275
300
charge (ADC counts)
ID 1
Entries 64000
Mean 187.0
RMS 36.78
counts
6000
5000
4000
3000
2000
1000
0
100
125
150
175
200
225
250
275
300
charge (ADC counts)

Figure 3

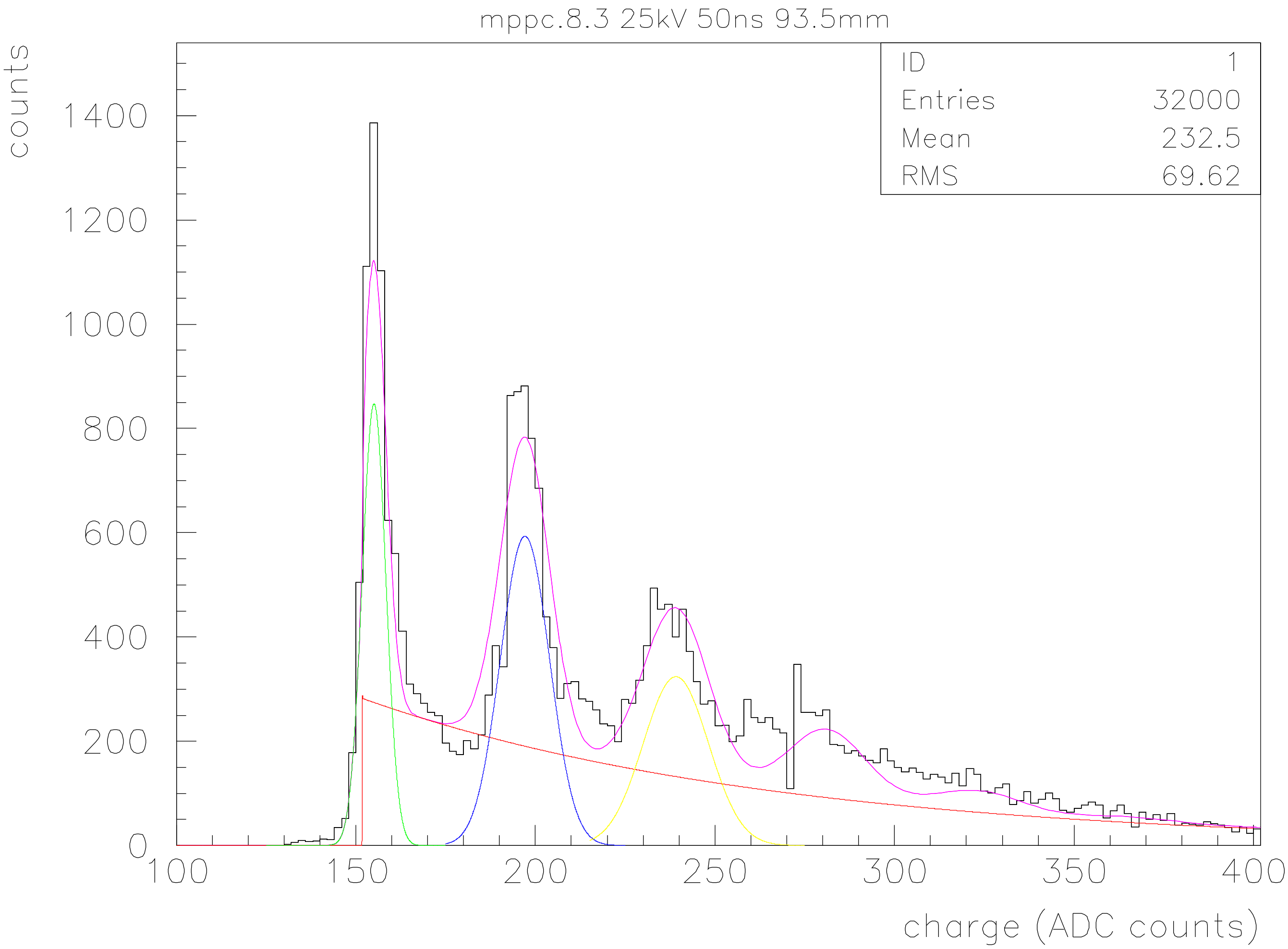
mppc.8.3 25kV 50ns 93.5mm
ID 1
Entries 32000
Mean 232.5
RMS 69.62
counts
0
200
400
600
800
1000
1200
1400
100
150
200
250
300
350
400
charge (ADC counts)

Figure 4

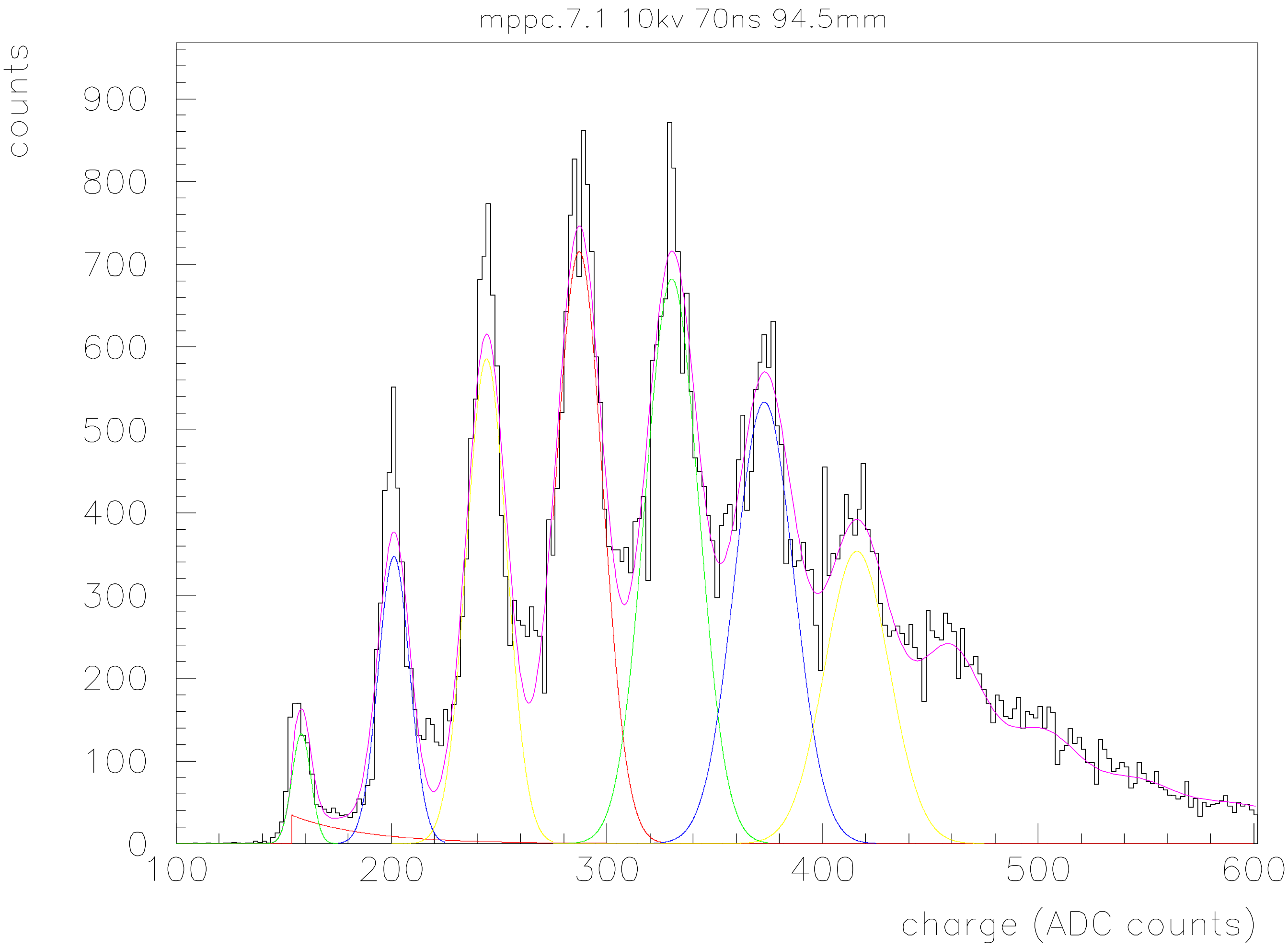

mppc.7.1 10kv 70ns 94.5mm
counts
900
800
700
600
500
400
300
200
100
0
100
200
300
400
500
600
charge (ADC counts)

Figure 5

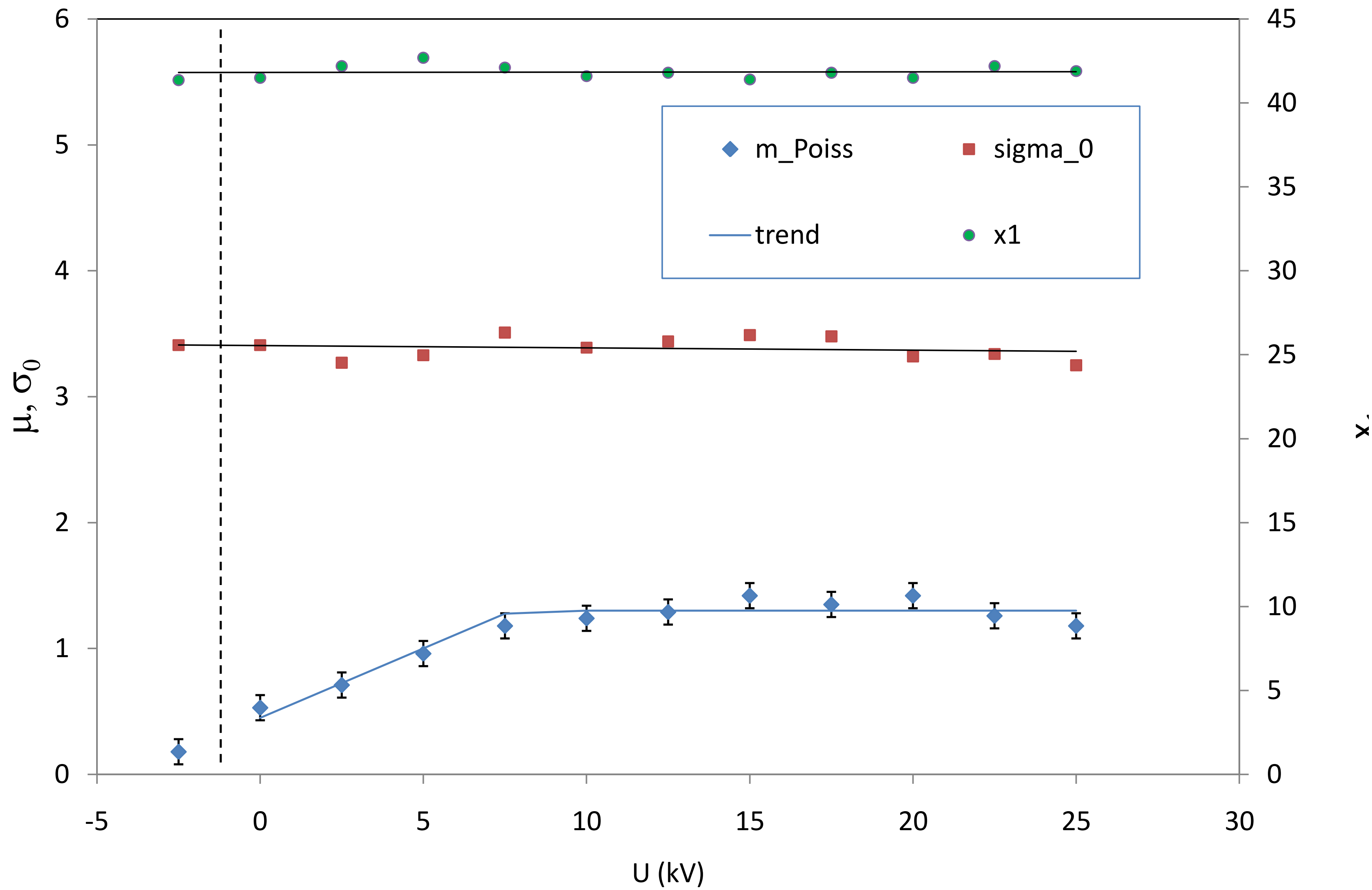

m_Poiss
sigma_0
trend
x1
μ, σ0
x
U (kV)
6
5
4
3
2
1
0
45
40
35
30
25
20
15
10
5
0
-5
0
5
10
15
20
25
30

Figure 6

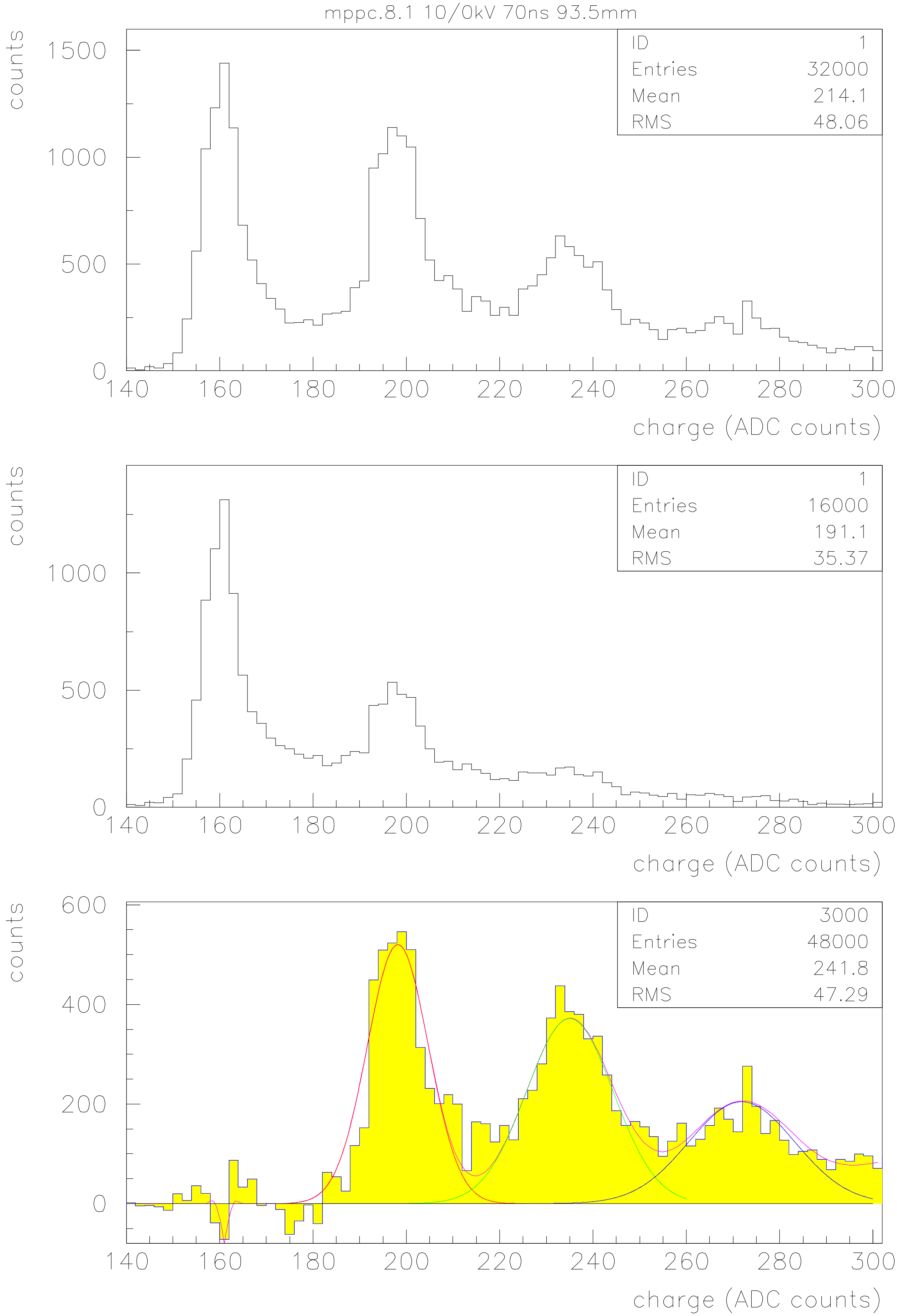

mppc.8.1 10/0kV 70ns 93.5mm
counts
ID 1
Entries 32000
Mean 214.1
RMS 48.06
1500
1000
500
0
140 160 180 200 220 240 260 280 300
charge (ADC counts)
counts
ID 1
Entries 16000
Mean 191.1
RMS 35.37
1000
500
0
140 160 180 200 220 240 260 280 300
charge (ADC counts)
counts
ID 3000
Entries 48000
Mean 241.8
RMS 47.29
600
400
200
0
140 160 180 200 220 240 260 280 300
charge (ADC counts)

Figure 7
Click here to download high resolution image